Available online at www.sciencedirect.com

ScienceDirect

Ceramics International 40 (2014) 2201–2208

CERAMICS INTERNATIONAL

www.elsevier.com/locate/ceramint

Studies of dielectric, pyroelectric and conduction mechanism of $Sr_3Ta_2O_8$

Biswajit Pati[a,b], R.N.P. Choudhary[a,*], Piyush R. Das[a]

[a]Department of Physics, Institute of Technical Education and Research, SOA University, Bhubaneswar 751030, India
[b]Department of Physics, Government Junior College, Bhawanipatna, Kalahandi 766001, India

Received 20 June 2013; received in revised form 21 June 2013; accepted 28 July 2013
Available online 13 August 2013

Abstract

The current research work reports on structural, dielectric, pyroelectric and conduction properties of strontium orthotantalate, prepared by using a high-temperature solid-state reaction technique. Preliminary x-rays structural study of the material confirms the formation of a single-phase compound with trigonal crystal structure. The microstructure of gold-coated pellet sample recorded by scanning electron microscopy (SEM) shows well-defined and homogeneously distributed grains. Detailed studies of dielectric parameters (ε_r and tan δ) of the compound as a function of temperature at some selected frequencies reveal that these parameters are invariant in a wide range of frequency and temperature (room temperature to about 400 °C). Studies of pyroelectric properties reveal that the materials have reasonably high figure of merit useful for fabrication of pyroelectric detector. The ac conductivity spectra show a typical-signature of an ionic conducting system, and are found to obey Jonscher's universal power law. The low leakage current and negative temperature coefficient of resistance (NTCR) behavior of the sample have been verified from $J \sim E$ plots. The nature of variation of dc conductivity with temperature confirms the Arrhenius and NTCR behavior in the material.

Keywords: B. X-ray methods; C. Dielectric properties; C. Electrical conductivity; D. Alkaline earth oxides

1. Introduction

The discovery of unusual non-linear properties (ferroelectricity) and other allied phenomena in Rochelle salt [1] in 1921, and later on barium titanate ($BaTiO_3$) of perovskite family have drawn the attention of researchers to search for new dielectric materials of different structural families for possible industrial applications. Some simple and complex oxides (derived from perovskite structure) were extensively investigated in order to search materials with structural stability [2,3], high dielectric constant, low dissipation factor, high quality factor, frequency and temperature independent dielectric properties useful for meaningful devices such as resonator, oscillator, filter for wireless communications and ferroelectric related devices [4–8]. In the process several lead based perovskites such as $Pb(ZrTi)O_3$ (PZT), $Pb(MgNb)O_3$ (PMN) etc. were found to have excellent dielectric, ferroelectric and pyroelectric properties useful for multilayer capacitors, sensors and actuators [9–12]. However, these lead based ceramics exhibits compositional fluctuations due to evaporation of PbO. As a result, the mechanical and electrical properties of these materials are greatly affected and create environmental pollution.

In order to solve these problems, non-toxic oxides (orthometallates) of alkaline earth metals with a general formula $A_3(BO_4)_2$ (A=divalent metal and B=pentavalent metal) have attracted much attention of material scientists to work on their structural, transport and ferroelectric properties for solid-state devices including lasers [13,14]. Among various metal oxides studied so far, only a few Ta-based perovskites such as $Ba_3MTa_2O_9$ (M=Zn, Mg) were found to have some interesting dielectric properties (i.e., low dielectric constant and low loss (10^{-5} at 1 GHz)) for micro-wave applications [15–18]. In this context some of the complex systems such as $MO–B_2O_5$ (M=Ba, Sr, Ca and B=V, Nb, Ta) binary system with different cationic ratio (M: B) have been found useful for devices. With the cationic ratio (M: B) as 3:1, the oxygen-deficient cubic (MO_2) layers are formed which forces a change in coordination

*Corresponding author. Tel.: +91 8763425977.
E-mail address: crnpfl@gmail.com (R.N.P. Choudhary).

0272-8842/$ - see front matter © 2013 Elsevier Ltd and Techna Group S.r.l. All rights reserved.
http://dx.doi.org/10.1016/j.ceramint.2013.07.138

of the B atoms from octahedral to tetrahedral. As a result, the palmierite structure can be derived from that of the 9R polytypes structures [19]. The investigation on the SrO-rich part of the $SrO–Ta_2O_5$ binary system (i.e., $Sr_3Ta_2O_8$) structure reveals that the inter-layer site of the Sr^{2+} cation is half occupied with a random distribution of vacancies. The defect structure and the presence of Ta^{5+} ions account for its high-temperature ferroelectric [20] and high-electronic conductivity [21,22]. Further, study on such compounds reveals that they decompose at ambient atmosphere and temperature because of their compositional variation with experimental conditions.

Detailed literature survey reveals that such metal orthotantates have many potential applications. Graham et al. [23] reported the crystal chemistry of complex niobium and tantalum oxides. Yan et al. [24] reported the electrical properties of ferroelectric–gate FETs with $SrBiTa_2O_9$, fabricated using MOCVD technique. Recently Li et al. [25] reported the photo-induced-topotactic growth of bismuth nanoparticles. The phase transition and piezoelectric properties of $SrBiTa_2O_9$ was reported in Machado et al. [26]. Senthil et al. [27] reported the impedance and electrical modulus study of microwave sintered $SrBiTa_2O_9$ ceramic. Goel et al. [28] reported the effect of annealing on the microstructure and PE hysteresis of vanadium doped $SrBiTa_2O_9$. It is very much clear from the above and other relevant-literatures (bismuth modified tantalum oxides), not much work has been reported on dielectric and pyroelectric properties of $Sr_3Ta_2O_8$.

Recently, we have reported the structural and electrical properties of $Ba_3V_2O_8$ and $Ba_3Nb_2O_8$ [29,30] compounds of this family. In view of the importance of the material for possible device applications, we have synthesized lead-free complex perovskite, $Sr_3Ta_2O_8$, by a standard solid-state reaction route and studied its dielectric, pyroelectric and conduction properties of the material, and reported here.

2. Materials and methods

The lead-free polycrystalline ceramic $Sr_3Ta_2O_8$ was prepared by the standard (mixed oxide) technique using the following chemical reaction: $3(SrCO_3)+Ta_2O_5 \rightarrow Sr_3Ta_2O_8+3(CO_2)$. The high purity (AR grade) precursors; $SrCO_3$ (99%, M/s LOBA Chemie Pvt. Ltd., India) and Ta_2O_5 (99.9%, M/s LOBA Chemie Pvt. Ltd., India), taken in proper stoichiometry, were mixed first mechanically in an agate-mortar and pestle for an hour followed by wet grinding (in methanol) for another hour to get a homogeneous mixture of the constituents. This mixture was finally calcined at 1425 °C (as decided by repeated firing/mixing) for 4 h in air. The formation and quality of the desired compound were checked from the X-ray diffraction (XRD) pattern of the material, recorded at room temperature using a X-ray powder diffractometer (XPERT-PRO, DISIR) with CuK_α radiation (λ=1.5405 Å) in a wide range of Bragg angle θ ($0 \le 2\theta \le 60$) at a scanning rate of 2°/min and comparing the same with that of JCPDS data. The calcined powder of the compound was cold pressed into cylindrical pellets (10 mm diameter and 1–2 mm thickness) using polyvinyl alcohol (PVA) as the binder and applying an isostatic pressure of 4×10^6 N/m^2. The pellets were then sintered in oxygen atmosphere at an optimized temperature 1450 °C for 4 h followed by natural cooling. To perform electrical measurements, both the flat and parallel surfaces of the sintered pellet were electroded with air-drying conducting silver paste and then dried at 150 °C for 8 h to remove moisture (if any). The dielectric and other related parameters were measured as a function of temperature (30–500 °C), at an input ac signal of small voltage amplitude (~1 V), over a wide range of frequencies (100 Hz–1 MHz) using a computer-controlled phase sensitive meter (PSM LCR 4NL, Model: 1735, UK) with a laboratory-designed and fabricated sample holder and a small vertical pit furnace. The polarization (hysteresis loop) of the poled sample (electric field=7 kV/cm, time=8 h) was obtained at different temperatures using a workstation of hysteresis loop tracer (M/S Marine India, New Delhi). The pyroelectric current of the pellet sample was measured at different temperature (30–500 °C) by an electrometer (KEITHLEY INSTRUMENTS INC., MODEL 6517B) at the heating rate of nearly 2°C/min. A constant voltage was applied across the sample to measure the dc conductivity using the same electrometer.

3. Results and discussion

3.1. Structural properties

Fig. 1 shows the room temperature XRD pattern of $Sr_3Ta_2O_8$ calcined powder. The diffraction pattern consists of a number of sharp peaks that are different from those of the ingredients. This pattern reveals better homogeneity and crystallization of the material, and thus confirming the formation of a new polycrystalline single-phase compound. The well-resolved sharp peaks of $Sr_3Ta_2O_8$ indicate the material is highly crystallized. All observed diffraction peaks of the pattern could be assigned to the trigonal phase which is in good agreement with the crystallographic data of similar type of compound $Sr_3V_2O_8$ (JCPDS: 81-1844) [13,31]. The lattice parameters of the selected unit cell were refined using the least-squares subroutine of the standard computer program package "POWD" [32]. These refined lattice parameters are: a=8.7225(4) Å and c=14.330(3) Å (the number in the parenthesis is estimated as standard deviation of unit cell parameters). Using refined lattice parameters, each peak was again indexed, and interplanar

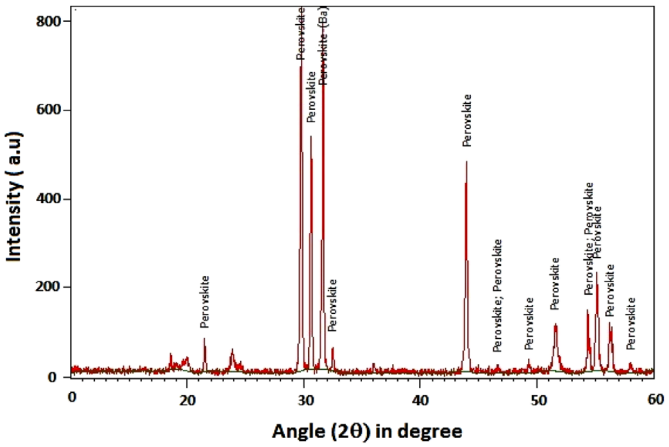

Fig. 1. XRD pattern of $Sr_3Ta_2O_8$ at room temperature.

spacing (d) of reflection planes of the compound was calculated, and compared with its observed value (Table 1). It is found that refined unit cell parameters with proposed crystal structure (trigonal) of the sample are very much consistent with that of similar types of compounds reported earlier [13,31,33]. As the powder sample was used to record XRD pattern, contributions of strain and other effects in the broadening of XRD peaks and crystallite size calculation have been ignored.

Fig. 2 shows the SEM micrograph of the sintered pellets recorded at room temperature. The micrograph shows a well-defined and homogeneous morphology for the sample. In spite of sintering at optimized high- temperature, some voids of irregular shape and dimension are still observed. Most of the grains have dimension in the range of ~2–5 μm.

3.2. Dielectric properties

Fig. 3 shows the temperature dependence of relative permittivity (ε_r) and loss tangent (tan δ) of $Sr_3Ta_2O_8$ with temperature at some selected frequencies (20, 100 and 1000 kHz). It reveals that the values of both ε_r and tan δ decrease on increasing frequency, which is a general feature of dielectric materials [34]. For a given frequency the value of ε_r is almost constant in the low and medium temperature ranges (from room temperature to 450 °C). On further increase in temperature, it increases gradually. At higher temperatures, the increase of ε_r (at lower frequencies) may be due to space charge polarization which arises from mobility of ions and imperfections in the material. These combined effects produce a sharp increase in the relative permittivity on increasing temperature. The value of relative permittivity at 450 °C for frequencies 20, 100 and 1000 kHz are 244, 238 and 227 respectively. As the compound exhibits frequency independent transition temperature (i.e., no dispersion), the material is of non-relaxor type. The relative permittivity or dielectric constant of the material decreases with rise in frequency because their dipolar and ionic polarizations decrease with rise in frequency. The defect structure along with the presence of Ta^{5+} ions accounts for its high-temperature ferroelectrics [35].

Table 1
Comparison of d_{obs}, d_{cal} and h k l values of all the reflections of XRD peaks.

Sl. no.	2θ (deg.)	d-spacing		Rel. int.(I/I_0)	Miller indices		
		d_{obs}	d_{cal}		h	k	l
1	21.49	4.1314	4.1312	8	2	1	1
2	23.81	3.7339	3.7337	5.4	3	0	1
3	29.72	3.0034	3.0014	100	3	0	2
4	30.58	2.9209	2.9232	65	4	0	1
5	31.58	2.8307	2.8308	99	1	0	3
6	32.47	2.7551	2.7683	6.5	2	2	2
7	43.93	2.0593	2.0573	59	2	0	4
8	46.62	1.9465	1.9476	1.4	5	2	1
9	49.31	1.8465	1.8455	1.9	3	3	3
10	51.55	1.7714	1.7729	12	7	0	0
11	54.35	1.6865	1.6854	17	6	0	3
12	55.09	1.6656	1.6701	27	4	3	3
13	56.21	1.6351	1.6351	11	2	1	5
14	57.99	1.5890	1.5890	2.1	5	4	0

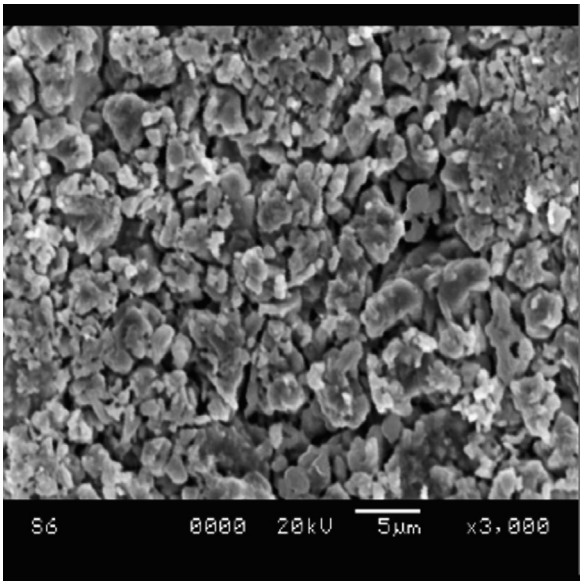

Fig. 2. SEM of $Sr_3Ta_2O_8$ at room temperature.

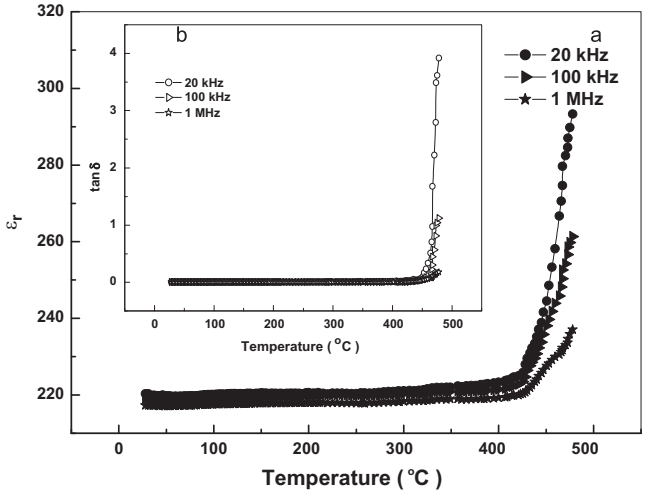

Fig. 3. Variation of ε_r and tan δ of $Sr_3Ta_2O_8$ with temperature at various frequencies.

Fig. 3 (inset) shows that the value of tan δ increases with rise in temperature. The rate of increase in tan δ in the material in the low-temperature region is slow, whereas at higher temperatures it increases sharply. This sharp increase in tan δ at higher temperatures may be due to (i) scattering of thermally activated charge carriers, (ii) some inherent defects in the sample and (iii) creation of oxygen vacancies during sample preparation. At higher temperatures the conductivity begins to dominate, which in turn, is responsible for rise in tan δ. Again, the dispersion in tan δ at higher temperatures, an important characteristic of normal ferroelectric material, may be attributed to non-negligible ionic conductivity in the material arising due to loss of oxygen during sintering at high temperatures. The compound shows very low loss (i.e., even at a temperature as high as 450 °C the value of tan δ is 0.098 at 20 kHz), which decreases further on increasing frequency (i.e., 0.044 at

100 kHz and 0.036 at 1 MHz). Due to very low loss the quality factor of the material is high.

In order to examine the effect of space charge polarization in the low-frequency range at high temperatures, we have plotted the real and imaginary part of dielectric constant (i.e., ε', ε'') with frequency at different temperatures. Fig. 4 shows the variation of ε' and ε'' with frequency above 300 °C. There is a sharp decrease in value of ε' and ε'' in the lower frequency region and showing a frequency independent value of these parameters in the high frequency region. The strong decrease of real and imaginary part of dielectric constant towards low frequency range may be due space charge polarization and interface effect.

3.3. Pyroelectric study

Ferroelectric materials, a sub-group of pyroelectric materials, exhibit temperature dependent spontaneous electric polarization, (i.e., polarization that changes with temperature) [36]. Pyroelectric current (I), developed on the surface of the material sample, can be calculated using the relation: $I = \Gamma A\, dT/dt$ where A is the area of the sample, Γ is the pyroelectric coefficient and dT/dt denotes the time rate of change of temperature of the material. Like relative permittivity (ε_r) the value of pyroelectric current increases with rise in temperature for $Sr_3Ta_2O_8$, and so also its pyroelectric coefficient (Fig. 5(a)). The value of pyroelectric coefficient at a temperature of 400 °C is found to be 1.11×10^4 μC m^{-2} °C^{-1} which is quite high as compared to that of earlier reported ones on some single crystals and/or ceramics such as $LiNbO_3$ (83 μC m^{-2} °C^{-1}), $Pb_5Ge_3O_{11}$ (110 μC m^{-2} °C^{-1}), $Ba_3Nb_2O_8$ (105 μC m^{-2} °C^{-1}), $PbTiO_3$ (180 μC m^{-2} °C^{-1}), SBN-50 (550 μC m^{-2} °C^{-1})etc. [37]. The higher pyroelectric coefficient of the sample reflects the good stoichiometry. Again, the nature of temperature dependence of pyroelectric current plot along with the absence of pyroelectric anomaly supports the nature of dielectric study in the material [38].

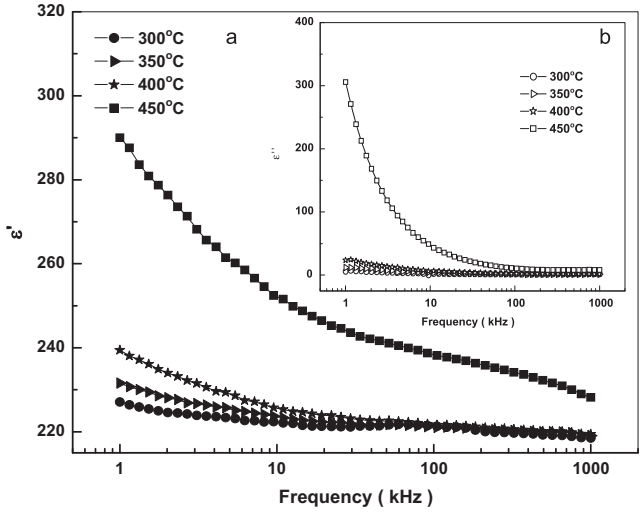

Fig. 4. Variation of ε' and ε'' with frequency at different temperatures.

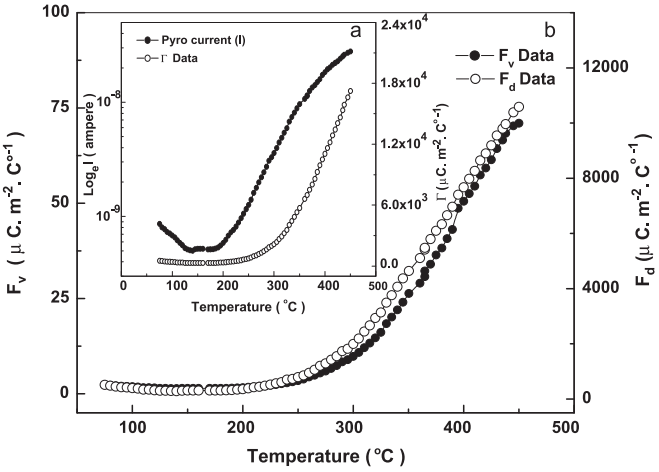

Fig. 5. Temperature dependence of (a) pyroelectric current and pyroelectric coefficient and (b) figure of merits (F_V and F_d) of $Sr_3Ta_2O_8$.

Pyroelectric figure of merits such as voltage responsivity (F_v) and detectivity (F_d) are important parameters to evaluate the utility of the materials for their heat sensing applications [38]. A pyroelectric detector requires high values of figure of merits. To achieve maximum performance of the device, the pyroelectric material must have a high pyroelectric coefficient and a small dielectric constant as well as tangent loss. The voltage responsivity is generally defined and calculated by using the following expression [39,40], $F_v = \Gamma/\varepsilon_r$Where, ε_r is the relative permittivity of the material. When tan δ is the dominant noise source associated with the pyroelectric material, the detectivity is evaluated as per the relation, $F_d = \Gamma/\sqrt{\varepsilon_r \tan\delta}$.

The efficiency or figures of merits is calculated from pyroelectric coefficient, dielectric constant and tan δ at 100 kHz using the above formula. The variation of F_v and F_d with temperature (Fig. 5(b)) suggests that the material have relatively high voltage responsivity and detectivity as compared to some reported compounds [37] that may be due to space charge effect or some other intrinsic charge carriers. This material is expected to be useful for pyroelectric detector with fairly high efficiency well above room temperature.

3.4. Polarization study

Fig. 6 shows the hysteresis loops of $Sr_3Ta_2O_8$ at room temperature. From the plot the values of remnant polarization ($2P_r$) and coercive field (E_c) were found to be 9.22 μC/cm^2 and 1.54 kV/cm at room temperature (30 °C) respectively. The nature of the loop at room temperature suggests the existence of ferroelectric properties in the material.

3.5. Relaxation time analysis

The complex impedance spectroscopy (CIS) is a useful technique to study the ac response of a system to a sinusoidal perturbation, and subsequent calculation of impedance and related parameters as a function of frequency at different temperatures [41–43].

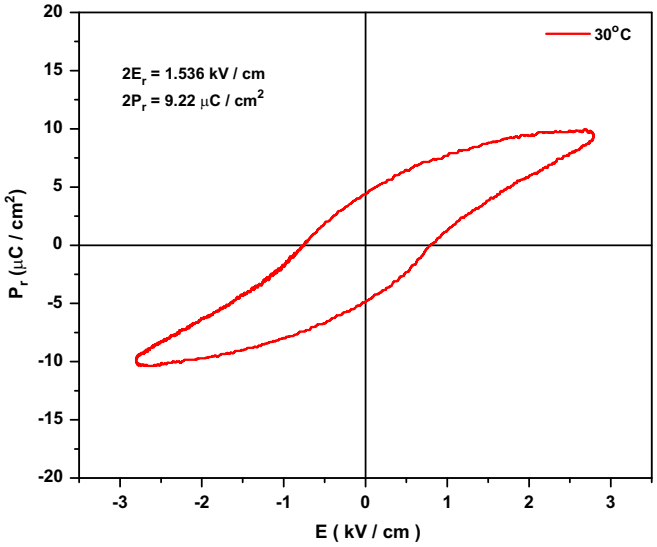

Fig. 6. Hysteresis loop of $Sr_3Ta_2O_8$ at room temperature.

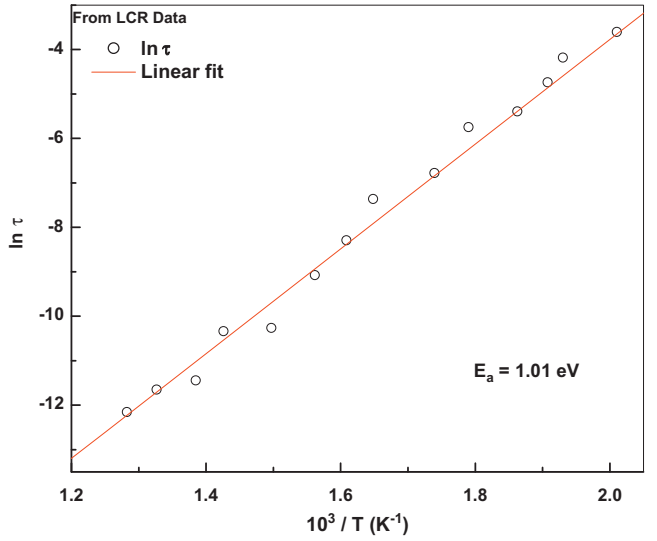

Fig. 7. Variation of relaxation time with inverse of absolute temperature.

The semi- circles in the impedance spectrum have a characteristic peak occurring at a unique relaxation frequency usually referred as resonance frequency (f_r) ($\omega_r=2\pi f_r$). The relaxation time due to bulk effect (τ) has been calculated using the equation $\omega_r R_b C_b=\omega_r\tau=1$ and thus $\tau=R_bC_b$.

Fig. 7 shows the variation of ln τ with inverse of absolute temperature (1000/T). The value of τ_b decreases with rise in temperature, and thus temperature dependent relaxation time for bulk follows the Arrhenius relation: $\tau=\tau_o\exp(-E_a/K_BT)$ where τ_o is the pre-exponential factor, K_B is Boltzmann constant and T is the absolute temperature. A careful comparison of temperature dependent bulk relaxation time with that of proposed model shows very good agreement indicating the validity of the model and accuracy of the experimental data. The calculated value of activation energy (E_a) was found to be 1.01 eV.

3.6. ac conductivity analysis

The ac conductivity of the sample can be calculated from the dielectric data using the relation: $\sigma_{ac}=\omega\varepsilon\varepsilon_0\tan\delta$, where $\varepsilon_0=$ absolute permittivity of free space and other parameters have their usual meanings. Fig. 8(a) shows the temperature dependence of σ_{ac} at some selected frequencies. The activation energy E_a (which is dependent on a thermally activated process) can be evaluated using an empirical relation: $\sigma_{ac}=\sigma_0\exp(-E_a/kT)$, where $k=$Boltzmann constant and $\sigma_0=$pre-exponential factor. For each frequency in the plot, occurrence of different slopes of different temperature-regions suggest the presence of multiple conduction mechanism in the sample with different activation energy [44]. The calculated activation energies (E_a) of the sample at frequencies 20 kHz, 100 kHz and 1000 kHz in low and medium temperature ranges are 0.28 eV, 0.14 eV and 0.02 eV respectively and the sharp increase in slopes at high temperatures indicates a considerable rise in conductivity and hence activation energy of the sample.

The phenomenon of the conductivity dispersion in solids is generally analyzed using Jonscher's power law; $\sigma_{ac}=\sigma_{dc}+A\omega^n$ where σ_{dc} is the dc conductivity at a particular temperature, A is temperature dependent constant and n is temperature dependent exponent in the range of $0<n<1$. The n represents the degree of interaction between mobile ions with the lattices around them, and A determines the strength of polarizability [44]. The frequency dependence of ac conductivity (σ_{ac} (ω)) at some selected temperatures is shown in Fig. 8(b). The conductivity curves show dispersion in the low-frequency region. From the graphs it is clear that σ_{ac} increases with rise in frequency but it is nearly independent at low frequency. The high frequency dispersion has been attributed to the ac conductivity whereas the frequency independent plateau region corresponds to the dc conductivity. The increasing trend of σ_{ac} with rise in frequency in lower frequency region may be attributed to the disordering of

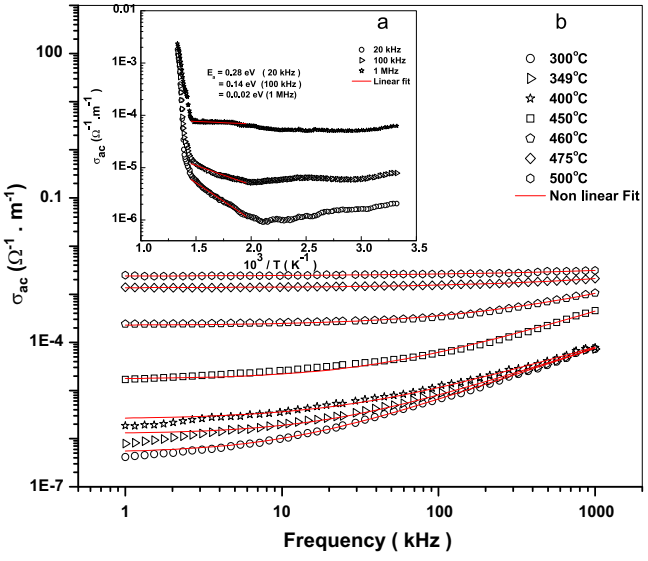

Fig. 8. (a) Variation of σ_{ac} of $Sr_3Ta_2O_8$ with inverse of absolute temperature at various frequencies. (b) Variation of σ_{ac} of $Sr_3Ta_2O_8$ as a function of frequency at various temperatures.

cations between neighboring sites, and presence of space charge [45]. In the high frequency-region the curves approach each other.

Jonscher attributed the origin of the frequency dependence of conductivity to the relaxation phenomena arising due to mobile charge carriers [46]. When a mobile charge carrier hops to a new site from its original site, it remains in a state of displacement between two potential energy minima. Also, the conduction behavior of the materials obeys the power law; $\sigma(\omega)\ \alpha\ \omega^n$ with a slope change governed by n in the low temperature region. The value of n less than 1 signifies that the hopping process involves a translational motion with a sudden hopping of charge carriers whereas $n>1$ means that the motion involves localized hopping without the species leaving the neighborhood [29]. The frequency at which change in slope takes place is known as hopping frequency of the polarons (ω_p), and is temperature dependent. The material obeys universal power laws and is confirmed by a fitting of above equation to the experimental data also shown in Fig. 8 (b). From non-linear fitting it is found that that motion of charge carriers is translational because of small value of n (<1) [47].

3.7. J–E characteristics and dc conductivity analysis

Fig. 9 shows the nature of dependence of current density (J) of the material upon applied field (E) at some selected temperatures. This $J\sim E$ study on ferroelectric ceramics is one of the useful characterization techniques to understand the conductivity mechanism in the sample. At a given temperature, the non-ohmic behavior of J–E graphs indicates the semiconducting nature of the material. The increase in slope of characteristic curves with rise in temperature suggests an increase in conductivity of the material and thus confirms its NTCR-type behavior. Further, the curves also reveal that the material allows a very small leakage current to pass through it.

Fig. 10(a) and (b) show the temperature dependence of dc conductivity of the material, obtained directly from LCR data using the relation: $\sigma_{dc}=t/R_bA$ where the symbols have their usual meanings and that from σ_{ac} fitting data respectively. The nature of these plots and the activation energy are consistent, and also are in good agreement with each other. The increase in the value of σ_{dc} with temperature supports the NTCR behavior of the sample. The nature of the plot follows the Arrhenius relation: $\sigma_{dc}=\sigma_0\exp(E_a/K_BT)$ [48]. The occurrences of different slopes at different temperature regions suggest the presence of multiple conduction processes in the sample with different activation energies [44,47]. The calculated values of activation energy (E_a) of the sample in medium (200–300 °C) and high-temperature range (400–500 °C) are 0.42 eV and 1.71 eV respectively. The small value of E_a suggests that the material can be activated by applying a relatively small energy. Also, the difference in the value of activation energy in the low and high temperature ranges supports the hopping-type conduction mechanism in the material [49]. Further, the mismatching of the values of E_a from the conductivity and relaxation time plots indicates that the charge carriers responsible for conduction and relaxation process are different.

4. Conclusion

In summary, the present study reports a novel approach to synthesize lead-free ceramic $Sr_3Ta_2O_8$, with a trigonal crystal structure at room temperature. The surface morphology of the compound, studied by SEM, shows homogeneously distributed grains. The dielectric study reveals that the material has moderate permittivity very low loss even at high temperature. Due to low loss the quality factor of the material is high. The moderate permittivity, low dielectric loss and high quality factor make this material (with suitable modifications) useful for high frequency applications. The electric polarization study along with the nature of hysteresis loop at room temperature suggests the existence of ferroelectricity in the material. The high value of pyroelectric coefficient and figure of merits suggests that the material can be useful for pyroelectric detectors. The frequency dependence of ac conductivity obeys

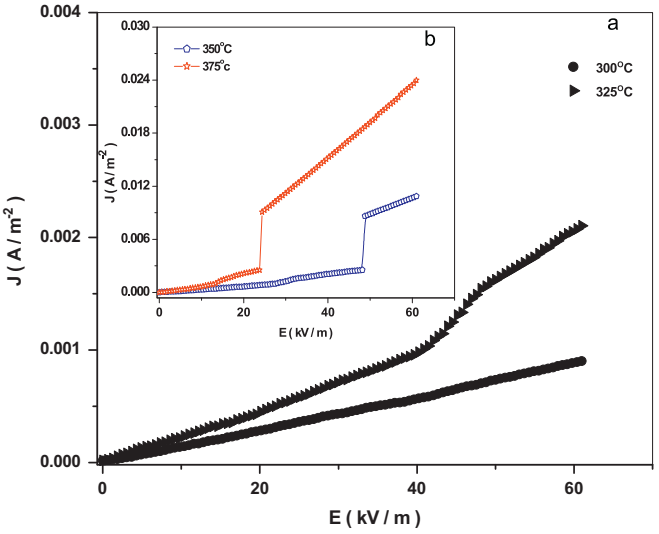

Fig. 9. J–E characteristics of $Sr_3Ta_2O_8$ at various temperatures.

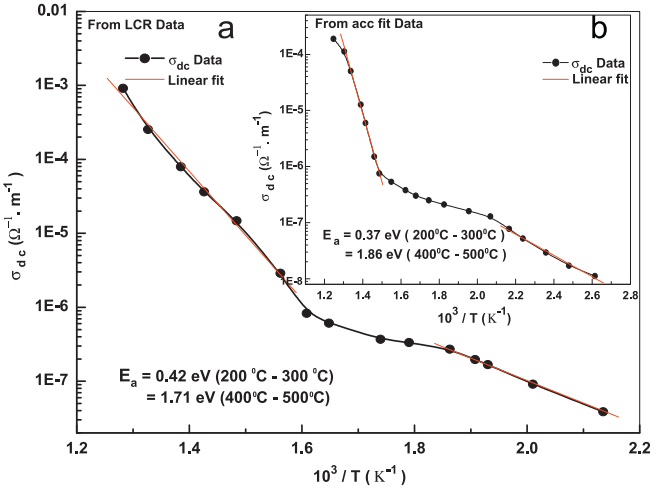

Fig. 10. Variation of σ_{dc} of $Sr_3Ta_2O_8$ with inverse of absolute temperature (a) from LCR data and (b) from σ_{ac} fit data.

Jonscher's universal power law. The dc conductivity study reveals that the material has semiconducting nature (NTCR behavior) with low leakage current and the nature of plot follows Arrhenius relation. The smaller value of dc activation energy suggests the conduction mechanism can be initiated in the material by applying a small amount of energy. The mismatching of activation energy of the sample, estimated from the conductivity plot and relaxation time plot, suggests that the charge carriers responsible for conduction and relaxation process are different.

Acknowledgments

The authors would like to acknowledge the kind help of Dr. B. Mishra, Principal Scientist, Dalmia Institute of Scientific and Industrial Research (DISIR), Rajgangpur, Odisha and IIT Kharagpur in carrying out some experimentation.

References

[1] J. Valsek, Piezo-electric and allied phenomena in Rochelle salt, Physical Review 17 (4) (1921) 475.
[2] K. Uchino, Ferroelectric Devices, Marcel Dekker Inc., New York, 2000.
[3] M.E. Lines, A.M. Glass, Principle and Application of Ferroelectrics and Related Materials, Clarndon Press, Oxford, 1977.
[4] D. Szwagierczak, J. Kulawik, Thick film capacitors with relaxor dielectrics, Journal of the European Ceramic Society 24 (2004) 1979.
[5] H. El Alaoui-Belghiti, R. Von der Mühll, A. Simon, M. Elaatmani, J. Ravez, Relaxor or classical ferroelectric behavior in ceramics with composition $Sr_{2-x}A_{1+x}Nb_5O_{15-x}F_x$ (A=Na, K), Materials Letters 55 (2002) 138.
[6] N. Wakiya, J.K. Wang, A. Saiki, K. Shinozaki, N. Mizutani, Synthesis and dielectric properties of $Ba_{1-x}R_{2x/3}Nb_2O_6$ (R: rare earth) with tetragonal tungsten bronze structure, Journal of the European Ceramic Society 19 (1999) 1071.
[7] J.E. Geusic, H.J. Levinstein, J.J. Rubin, S. Singh, L.G. Van Uitert, The nonlinear optical properties of $Ba_2NaNb_5O_{15}$, Applied Physics Letters 11 (1967) 269.
[8] J.J. Rubin, L.G. Van Uitert, H.J. Levinstein, The growth of single crystal niobates for electro-optic and non-linear applications, Journal of Crystal Growth 1 (1967) 315.
[9] L.H. Brixner, P.L. Flournoy, Calcium orthovanadate $Ca_3(VO_4)_2$ – a new laser host crystal technical papers, Journal of The Electrochemical Society 112 (1965) 303.
[10] A. Grzechnik, P.F. McMillan, In situ high pressure raman spectra of $Ba_3(VO_4)_2$, Solid State Communications 102 (1997) 569.
[11] L.D. Merkle, A. Pinto, H. Verdun, B. McIntosh, Laser action from Mn^{5+} in $Ba_3(VO_4)_2$, Applied Physics Letters 61 (1992) 2386.
[12] B. Buijsse, J. Schmidt, I.Y. Chan, D.J. Singel, Electron spin-echo-detected excitation spectroscopy of manganese doped $Ba_3(VO_4)_2$: identification of tetrahedral Mn^{5+} as the active laser center, Physical Review B 51 (1995) 6215.
[13] P. Parhi, V. Manivanan, S. Kohli, P. McCurdy, Synthesis and characterization of $M_3V_2O_8$ (M=Ca, Sr and Ba) by a solid-state metathesis approach, Bulletin of Materials Science 31 (6) (2008) 885.
[14] A.M. Glass, S.C. Abrahams, A.A. Ballmann, G. Laiacono, Calcium orthovanadate, $Ca_3(VO_4)_2$ – a new high-temperature ferroelectric, Ferroelectrics 17 (1978) 579.
[15] S. Kawashima, M. Nishida, I. Ueda, H. Ouchi, $Ba(Zn_{1/3}Ta_{2/3})O_3$ ceramics with low dielectric loss at microwave frequencies, Journal of the American Ceramic Society 66 (1983) 421.
[16] S.B. Desu, J.M. O′Bryan, Microwave loss quality of $BaZn_{1/3}Ta_{2/3}O_3$ ceramics, J, American Ceramic Society 68 (1983) 546.
[17] L. Chai, P.K Davies, Formation and structural characterization of 1:1 ordered perovskites in $BaZn_{1/3}Ta_{2/3}O_3$–$BaZrO_3$ system, Journal of the American Ceramic Society 80 (1997) 3193.
[18] W. Wersing, Electronic Ceramics, in: B.C.H. Steele (Ed.), Elsevier, New York, 1991 (Chapter 4).
[19] R. Umemura, H. Ogawa, A. Yokoi, H. Ohsato, A. Kan, Low-temperature sintering-microwave dielectric property relations in $Ba_3(VO_4)_2$ ceramic, Journal of Alloys and Compounds 424 (2006) 388.
[20] E.G. Gonzalez, M. Parras, J.M.G. Calbet, Electron microscope study of a new cation deficient perovskite-like oxide: $Ba_3MoNbO_{8.5}$, Chemistry of Materials 10 (1998) 1576.
[21] B. Mossner, S.K. Sack, 9R- Stapelvarianten vom Typ $Ba_3(B, B')_2O_{9-y}$ mit B, B′=Mo, W, V, Ti, Journal of the Less Common Metals 114 (1985) 333.
[22] A. Grzechnik, Crystal structure of $Ca_3(VO_4)_2$ synthesized at 11 GPa and 1373 K, Solid State Sciences 4 (2002) 523.
[23] J. Graham, M.R. Thornber, The crystal chemistry of complex Niobium and Tantalum oxides: I. Structural classification of MO_2 phases, American Mineralogist 59 (1974) 1026.
[24] K. Yan, M. Takahashi, S. Sakai, Electrical properties of ferroelectric–gate FETs with $SrBiTa_2O_9$ formed using MOCVD technique, Applied Physics A 108 (2012) 835.
[25] Y. Li, L. Zang, Y. Liu, C. Liu, Z. Zhang, H. He, C. Wang, Photo-induced-topotactic growth of Bismuth nanoparticles from bulk $SrBiTa_2O_9$, Chemistry of Materials 25 (2013) 2045.
[26] R. Machado, M. Scpliarsky, M.G. Stachiotti, Phase transition and piezoelectric properties of $SrBiTa_2O_9$ by molecular dynamic simulations, Journal of Materials Science 45 (2010) 4912.
[27] V. Senthil, T. Badapanda, A.C. Bose, S. Panigrahi, Impedance and electrical modulus study of microwave sintered SrBiTa2O9 ceramic, in: ISRN Ceramics, vol. 2012, 6 p., Article ID 943734, 2012, http://dx.doi.org/10.5402/2012/943734.
[28] P. Goel, V.N. Ojha, K.L. Yadav, Effect of annealing on the microstructure and PE hysteresis of vanadium doped $SrBiTa_2O_9$, Materials Research Innovations 13 (3) (2009) 352.
[29] B. Pati, B.C. Sutar, P.R. Das, R.N.P. Choudhary, Dielectric and impedance spectroscopy of barium orthovanadate ceramics, Journal of Materials Science Materials in Electronics 24 (2013) 1608.
[30] B. Pati, R.N.P. Choudhary, P.R. Das, B.N. Parida, R. Padhee, Dielectric and impedance spectroscopy of barium orthoniobate ceramics, Journal of Electronic Materials 42 (2013) 1225.
[31] K.B. Shim, C.S. Lim, MAS synthesis and characterization of $Sr_3V_2O_8$ nanoparticles, Journal of Ceramic Processing Research 13 (2012) 291.
[32] E. Wu, POWD, an Interactive Powder Diffraction Data Interpretation and Indexing Program, Ver. 2.1, School of Physical Sciences, Flinders University South Bedford Park, SA 5042 Australia.
[33] A. Durif, Structure crystalline des orthovanadates et orthoarseniates de barium et de strontium, Acta Crystallographica 12 (1959) 420.
[34] J.C. Anderson, Dielectrics, Chapman & Hall, London, 1964.
[35] T.A. Vanderah, T.R. Collins, W. Wong-Ng, R.S. Roth, L. Farber, Phase equilibria and crystal chemistry in the Bao–Al_2O_3–Nb_2O_5 and Bao–Nb_2O_5 systems, Journal of Alloys and Compounds 346 (2002) 116.
[36] G.G Roberts, B. Holcroft, Thermal imaging using organic films, Thin Solid Film 180 (1989) 211.
[37] B.N. Parida, P.R. Das, R. Padhee, R.N.P. Choudhary, Phase transition and conduction mechanism of rare earth based tungsten-bronze compounds, Journal of Alloys and Compounds 540 (2012) 267.
[38] P. Ganguli, S. Devi, A.K Jha, Dielectric and pyroelectric studies of tungsten-bronze structured $Ba_5SmTi_3Nb_7O_{30}$ ferroelectric ceramics, Ferroelectrics 381 (2009) 111.
[39] R. Colbrook, G.G. Roberts, Pyroelectric Langmuir–Blodgett films incorporating metallic cations, Ferroelectrics 118 (1991) 199.
[40] M. Petty, J. Tsibouklis, F. Davis, P. Hodge, M.C. Petty, W.J. Feast, Pyroelectric Langmuir–Blodgett films prepared using preformed polymers, Journal of Physics D Applied Physics 25 (1992) 1032.
[41] S. Sen, R.N.P. Choudhary, Impedance studies of Sr modified $BaZr_{0.15}Ti_{0.95}O_3$ ceramics, Materials Chemistry and Physics 87 (2004) 256.

[42] S. Brahma, R.N.P. Choudhary, A.K. Thakur, AC impedance analysis of $LaLiMo_2O_8$ electroceramics, Physica B 355 (2005) 188.
[43] J.R. Macdonald, Impedance Spectroscopy Emphasizing Solid Materials and Systems, Wiley, New York, 1987 (Chapter-4).
[44] D.K. Pradhan, R.N.P Choudhary, C. Rinaldi, R.S. Katiyar, Effect of Mn substitution on electrical and magnetic properties of $Bi_{0.9}La_{0.1}O_3$, Journal of Applied Physics 106 (2009) 24102.
[45] R.N.P. Choudhary, D.K. Pradhan, C.M. Tirado, G.E. Bonilla, R.S. Katiyar, Effect of La substitution on structural and electrical properties of Ba $(Fe_{2/3}W_{1/3})O_3$ nanoceramics, Journal of Materials Science 42 (2007) 7423.
[46] A.K. Jonscher, The 'Universal' dielectric response, Nature 267 (1977) 673.
[47] D.K. Pradhan, B. Behera, P.R. Das, Studies of dielectric and electrical properties of a new type of complex tungsten bronze electroceramics, Journal of Materials Science Materials in Electronics 23 (2012) 779.
[48] J.R. Macdonald, Note on parameterization of the constant phase admittance element, Solid State Ionics 13 (1984) 147.
[49] Z. Lu, J.P. Bonnet, J. Ravez, J.P. Hagenmuller, Correlation between low frequency dielectric dispersion (LFDD) and impedance relaxation in ferroelectric ceramic $Pb_2KNb_4TaO_{15}$, Solid State Ionics 57 (1992) 235.